1 **Long-term trends of instability and associated parameters**
2 **over the Indian region obtained using radiosonde network**

3 Rohit Chakraborty, Madineni Venkat Ratnam* and Ghouse Basha

4 National Atmospheric Research Laboratory, India.

5 *Correspondence to:* M. Venkat Ratnam (vratnam@narl.gov.in)

7 **Abstract**

8   Long-term trends of the parameters related to convection and instability obtained from 27 radiosonde
9 stations across 6 sub-divisions over Indian region during the period 1980-2016 is presented. A total of 16 parcel
10 and instability parameters along with moisture content, wind shear, and thunderstorm and rainfall frequencies
11 have been utilized for this purpose. Robust fit regression analysis is employed on the regional average time
12 series to calculate the long-term trends on both seasonal and yearly basis. The Level of Free Convection (LFC)
13 and Equilibrium Level (EL) height is found to ascend significantly in all Indian sub-divisions. Consequently, the
14 coastal regions (particularly the western coasts) experience strengthening in Severe Thunderstorm (TSS) and
15 Severe Rainfall Frequencies (SRF) in the pre-monsoon while the inland regions (especially central India)
16 experience an increase in Ordinary Thunderstorm (TSO) and Weak Rain Frequency (WRF) during the monsoon
17 and post-monsoon. The 16-20 year periodicity is found to dominate the long-term trends significantly compared
18 to other periodicities and the increase in TSS, SRF and CAPE is found more severe after the year 1999. The
19 enhancement in moisture transport and associated cooling at 100 hPa along with dispersion of boundary layer
20 pollutants is found to be the main cause for the increase in Convective Available Potential Energy (CAPE)
21 which leads to more convective severity in the coastal regions. However, in inland regions moisture-laden winds
22 are absent and the presence of strong capping effect of pollutants on instability in the lower troposphere has
23 resulted in more Convective Inhibition Energy (CINE). Hence, TSO and weak rainfall occurrences have
24 increased particularly in these regions.

25 *Key words*: Instability, Convection, Long-term trends, Radiosonde

27 **1. Introduction**

28   Intense convective phenomena are a common climatic feature in the Indian tropical region which occurs
29 during the pre-monsoon to post-monsoon seasons (April–October) (Annanthakrishnan, 1977) and they are
30 generally accompanied by intense thunderstorms, lightning, wind gusts with heavy rainfall. Hence, they are
31 known to induce immense socio-economic hazards including loss of life and property. Several reports have
32 showed an increase in the climatic extreme occurrence and intensity of these phenomena throughout the world
33 (Emanuel, 2006; Webster et al., 2005). In this connection, the traditional surface-based parcel theory has been
34 utilized to understand convective processes using atmospheric soundings as it calculates the atmospheric
35 instabilities and other parameters at various heights (Huntrieser, 1997; Shanti et al., 2014, Nelli et al, 2018a).
36   Considering the importance of studying the long-term trends in climatic extremes, a series of research
37 attempts have been orchestrated world-wide in the last two decades. Using multiple tropical stations and re-

38   analysis data, Gettleman et al. (2002) and Reimann-Campe et al. (2009) has shown that Convective Available

39   Potential Energy (CAPE) has been increasing during the period 1958-1997 due to surface heating and moisture.

40   Gensini and Mote (2015) projected a 236 % increase in severe thunderstorm frequency over the eastern United

41   States (US). Further, Brooks (2013) used various combinations of CAPE and Vertical Wind Shear (VWSH)

42   products and results hinted towards a probable increase in the severe thunderstorms over the US. It was also

43   observed that the effect of increasing CAPE is more dominant on convective severity than in case of decreasing

44   shear. On the other hand, studies by Kharin et al. (2013), Trenbreth et al. (2003) and Prein et al. (2017) showed

45   that a recent increase of temperature has led to a rise of moisture ingress and consequently the frequency and

46   severity of extreme precipitations associated with intense convections have shown a steep rise everywhere in the

47   world. At the same time, an increase in thunderstorm severity and instability has also been reported by many

48   attempts over the Asian region (Wang et al., 2011; Saha et al., 2016).

49   Over Indian region, Manohar et al. (1999) studied the latitudinal variation and distribution of

50   thunderstorm frequency and CAPE and postulated that the temperature at 100 hPa has a strong relationship with

51   it. Dhaka et al. (2010) utilized radiosonde observations to support this hypothesis and arrived at similar

52   conclusions. Later, Murugavel et al. (2012) added to this hypothesis, stating that low-level moisture and solar

53   cycle also have additional impact on these phenomena. Recently, Chakraborty et al. (2017a) and Saha et al.

54   (2017) reported that lower instability is reducing at certain Indian stations due to pollution and global warming.

55   Apart from that, some studies have also attempted to correlate convective severity with boundary layer

56   phenomena, surface fluxes, solar effect and precipitation; (Murthy and Shivaramakrishnan, 2006; Allapattu and

57   Kunnikrishnan, 2009; Xie et al., 2011, Nelli et al. 2018b).

58   Previous studies over India has shown the distribution of CAPE only whereas other parameters like

59   Convective Inhibition Energy (CINE), Mixed Layer CAPE (MLC), Lifted Index (LI), Total Totals Index (TTI),

60   and Precipitable Water Vapor (PWV) are also important as they explain how the atmospheric instability and

61   moisture changes at various levels of the atmosphere. In addition, the influence of climatic oscillation (Quasi-

62   Biennial Oscillation (QBO), El-Nino Southern Oscillation (ENSO) and Solar Cycle) on the seasonal and annual

63   variation of convective parameters is also not studied in detail. Therefore in the present study, long-term

64   variation of parcel parameters (Lifted Condensation Level (LCL), Level of Free Convection (LFC), Equilibrium

65   Level (EL), CAPE and CINE), with instability (LI, Vertical Totals Index (VT)), moisture (PWV, and PWV at

66   low levels (PWL)), thunderstorm and rainfall severity frequencies (Thunder Storm-Severe (TSS), Thunder

67   Storm-Ordinary (TSO), Weak Rain Fall (WRF) and Strong Rain Fall (SRF)) followed by Temperature at

68   100hPa (T100) and Wind Shear (WSH) is investigated using 27 radiosonde stations along with gridded rainfall

69   data over India. This article is structured as follows: Section 2 describes the datasets and methodology adopted

70   for the present study. Section 3 presents the long-term analysis of parcel and instability parameter over Chennai

71   (13.08°N, 80.27°E) and 6 sub-divisions of the Indian subcontinent on both annual and seasonal basis, followed

72   by the periodicity and split trend analysis. Finally, a discussion on the results and conclusions is appended in

73   Section 4 and 5, respectively.

74

75   **2. Dataset and Methodology**

76   Radiosonde observations from 27 stations over Indian region from 1980-2016 are obtained from

77   Integrated Global Radiosonde Archives (Durre et al., 2006). These datasets provide daily temperature and

humidity profiles from 1538 stations around the world in fixed pressure levels after doing quality checks (Durre et al., 2006; Zhe et al., 2013). These studies have concluded that the radiosonde data quality from IGRA has faced certain problems from time to time, but such cases are not so prominent over the Indian region, especially after the year 1980. It is mainly because of the higher accuracy and reliability of this in-situ measurement technique that these datasets are widely used worldwide nowadays for calibrating other continuous profiler instruments (Chakraborty et al., 2016). In accordance with the above, we have considered only 27 stations out of 37 IGRA Indian radiosonde stations which provide a data availability of at least 8000 profiles in order to obtain statistically significant results. Note that the volume of usable radiosonde profiles for analysis at 00Z is found to be ~60-70% of the total number of days between (1980-2016) for all the IGRA stations. When an in depth investigation is done on the data continuity by plotting the temperature and humidity profiles for all days, a set of monthly gaps were discovered in the data. Most of the stations had 2-7 months gap but, leaving only two to three cases, the duration of these individual data gaps were mostly within 1 month. Since seasonal or annual average is used, hence in long term those small gaps were not found to be significant with respect to the total span of (37 years X 12 months).the data.

These 27 stations have been divided into six homogenous regions as defined by the India Meteorological Department (IMD) (Rao, 1976) which are: Central India (CI), East Coast (EC), North East (NE), North West (NW), Peninsula India (PI) and the West Coasts (WC) as shown in Fig. 1. Further, for simplicity, these regions have again been combined into three major categories namely: coastal regions (EC and WC), Inland (CI and PI) and others (NE and NW). Atmospheric profiles at 00Z have only been used in this analysis to preserve the maximum availability of data and to negate issues related to the diurnal variability of convection. Again, out of the available radiosonde profiles, some profiles have displayed absurd variations of temperature and humidity at various heights and hence they are discarded. A complete detail about the final dataset used for every station is indicated in Table A1. It may be noted here that the volume of observations are found to distributed almost homogenously throughout the measurement period and a detailed year wise breakup of radiosonde launches utilized are not shown to maintain the focus of the work. For calculation of the instability parameters, the temperature and humidity profiles were transformed from the standard pressure levels using cubic spline interpolation at every 100 m height bins. After this, a similar surface-based parcel method is utilized for estimating the parcel and instability parameters (LCL, LFC, EL, CAPE, MLC, CINE) as already described by Chakraborty et al. (2018). A small detail about the physical significance of these parameters is now given in Supplementary Section. For thunderstorm genesis, moisture growth and wind shear are extremely important, therefore we calculated the total amount of water vapor (PWV) and that upto 700 hPa level (PWL) along with the horizontal wind shear between surface and 6 km altitude. In addition to these, we have used temperature at the 100 hPa pressure level as it is found to strongly influence the convective strengths over the Indian region (Manohar et al., 1999; Dhaka et al., 2010).

Along with these parameters, the long-term impact of instability on the convection has also been studied from thunderstorm and rain frequencies. Daily measurements of surface wind speeds is obtained for all the radiosonde observations at 00Z using the Wyoming Website. The thunderstorm frequencies are calculated on yearly basis based on the criterion given by IMD. According to this criterion, if the maximum surfaces wind speed is greater than 62 km/h then it is considered as a severe thunderstorm event otherwise if wind speeds are between 31 and 62 km/h then it is considered as an ordinary thunderstorm case (also used by Saha et al. (2014)).

118 Hereafter, the total number of thunderstorm occurrences per year in both severe and ordinary category is
119 counted and represented by thunderstorm frequencies as TSS and TSO. In the same way, IMD provides daily
120 rainfall accumulations in 0.25 degree spatial resolution over the Indian region since the year 1900 (Rajeevan et
121 al., 2006, 2008; Pai et al., 2014). This daily precipitation data at the closest grid point is used to define the
122 frequency of severe and weak rainfall days. The severe rainfall frequencies constitute those days where the daily
123 accumulation is greater than 124.5 mm/day while for the weak rainfall cases it is less than 7.5 mm/day
124 according to IMD glossary as given in http://imd.gov.in/section/nhac/termglossary.pdf

125   From the previous section, it follows that a set of 14 parcel parameters with thunderstorm and rainfall
126 frequencies are essential to understand the convective climatology over India. But other than these, we also
127 require some important instability parameters. Hence, principle component analysis test is performed on the
128 total set of 8 well known instability parameters (LI, KI, TTI, CT and VT with CAPE, CINE, and MLC), as
129 already elaborated in previous attempts by Chakraborty et al. (2018) to identify the parameters that effectively
130 represents the variance of all the instability parameters. To do this analysis, daily datasets of all instability
131 parameters are averaged to yearly for every regions and then the principal components on the datsets are
132 obtained. The variance distribution plot (not shown) for each region showed that only the first two components
133 contribute to more than 70% of the total variance; hence the covariance scores of these two strongest orthogonal
134 components are plotted in Fig. 2 which depict that the LI is completely unrelated to rest of the parameters. Since
135 VT is found to lie exactly in the middle of the rest of the parameters, thus these two parameters can represent the
136 population in a convenient way.

137   Thus, a set of 16 parameters are finally taken for the analysis: LCL, LFC, EL, LI, VT, CAPE, CINE,
138 MLC, PWV, PWL, WSH, T100, TSO, TSS, WRF and SRF. However, apart from the IGRA radiosonde and the
139 IMD rainfall database, it was believed that some other parameters may also be externally responsible for the
140 changing trends in atmospheric instability and hence they are also included. They comprise the monthly mean
141 aerosol absorption index (AAI) data taken from the Tropospheric Emission Monitoring Internet Service
142 (TEMIS) Air Pollution Archive (De Graaf et al., 2005). In addition, the monthly average gridded data of ozone
143 mixing ratio (OMR) and Specific Humidity (SHUM) along with Downward Long Wave Radiation Flux
144 (DLWRF) are also utilized from ERA-Interim Re-analysis datasets.

145   We have estimated all parameters from daily radiosonde data and averaged over a season and annually
146 for obtaining trend at 95% confidence interval using robust regression analysis (Shepard, 1968). Further, the
147 parameters from radiosonde were averaged region wise and then the robust fit algorithm is employed on the
148 normalized time series to get the long-term trends (Anderson, 2008; Raj et al., 2018). These yearly trend values
149 are multiplied by 37 to get the total climatological trend in one parameter over the complete data span of 1980-
150 2016. For seasonal trend analysis, the same approach has been utilized for different seasons. The seasonal
151 distribution has been adopted from IMD reports which are as follows: Pre-monsoon (March-May), Monsoon
152 (June-September), Post-monsoon (October-November) and Winter (December-February). Further, for studying
153 the periodicities associated with each of these time series, an Empirical Mode Decomposition (EMD) technique
154 is used (Wu and Huang, 2009). Finally, the robust fit analysis is done on each of these components to compare
155 the trends from each periodicity to determine which of the periodicities dominates in each parameter.

156

157

3. Results

3.1. Climatic trends over Chennai

In the previous study by Chakraborty et al. (2018), long term trends of instability were investigated over Gadanki. To see whether, the observed trends of these parameters are behaving similarly in case of IGRA profiles also, in Fig.3 the climatic trends of instability are now described over Chennai (13.08^{o}N, 80.27^{o}E) which is the closest radiosonde station from Gadanki. A decreasing trend in VT, PWL and a strengthening of CINE with LI is noticed which indicates a reduction in the lower atmospheric instability (Fig.3d,e,h,i). However, CAPE (Fig.3f) shows significant increasing trends throughout the period. LFC has a slightly increasing trend (~18 hPa) which leads to increasing CINE and decreasing VT over Chennai, while the EL is found to get lifted up drastically (Fig.3c) resulting in an increase in the total instability and CAPE. The intensification in EL can be caused by a reduction in temperatures in the upper tropospheric heights (Manohar et al, 1999). Hence, it can be inferred that the reduction in temperatures near 100 hPa (Fig.3l) plays an important role in modulating the total atmospheric instability and CAPE.

The enhancement in CINE and reduction VT leads to the reduction in the frequency of weaker convective systems with medium or lower CAPE values. Again, as CAPE is one of most important parameters that modulate convective severity, hence the frequency of severe thunderstorms and heavy rainfall occurrences is expected to rise (Fig.3n,p). Thus, it is inferred that lower level instability has reduced due to elevated CINE and LFC; while the upper-level atmospheric instability has intensified significantly due to a cooling at 100 hPa and ascension in EL over Chennai. Hence, CAPE value increases drastically leading to more severe thunderstorm and heavy rainfall frequency events during the mentioned period.

Before proceeding to the investigation on the climatological trends of convection and instability over the Indian region, it is necessary to validate whether the obtained hypothetical trends from Chennai are free from any data quality issues. Hence a region wise climatology of the most important parameter CAPE is obtained from all the Indian regions using ERA-Interim Reanalysis data and the trends are shown in Fig. S1. This figure clarifies that all the Indian regions (especially the coastal regions) have experienced a common strengthening in CAPE especially after 1996-2000. Thus, the stated hypothesis looks clear and hence this can be progressed over a much broader way.

3.2. Climatological average of parameters

The climatological mean values of all instability parameters over six different Indian sub-divisions are shown with boxplot analysis in Fig. 4. The utility of using this approach is that, it will reveal which regions of India shows normal expected variation (if it lies within the box limits signifying 25-75% percentage of the distribution), while on the other hand it will also identify those regions having the extreme outlier values (lying outside the whiskers signifying the outermost 5% of the distribution). The LCL (Fig.4a) and LFC (Fig.4b) are found to be at the lowest altitudes in the coastal regions. As these stations receive most of the moisture from Sea, the EL (Fig.4c) is also expected to be higher in the coasts and lower elsewhere. However, due to low moisture availability, the inland regions experience weaker instability which results in lower CAPE (~900 J/kg) (Fig.4f) with higher CINE (Fig.4h) and WSH (Fig.4k). During strong convection, values of LI (Fig.4d) (which represents that the mid-tropospheric instability) are also higher in the coastal regions. Similarly, height integrals of instability such as CAPE (Fig.4f) and MLC (Fig.4g) are significantly higher (~1500 J/kg) in the coastal regions while the magnitude of MLC (Fig.4g) is found to be almost half of CAPE. As the trends in total

198 convective strengths below 300 hPa are quite low compared to that over the total atmospheric column, hence it
199 follows that the portion of buoyant column above 300 hPa must have contributed significantly to the total
200 convective developments over the Indian region. Again, being opposite of CAPE, CINE values are minimum in
201 the coastal regions compared to inland and continental regions thereby serving as a potential cause for the
202 reduced instability in these regions.

203 Similar to CAPE and MLC combination, the PWV (Fig.4i) and PWL (Fig.4j) pair shows the highest
204 averages in the coastal regions due to their closest proximity to the adjoining seas. Also, PWL (moisture integral
205 up to 700 hPa) is found to be almost half of PWV, hence the mid and upper tropospheric humidity is found to
206 play a strong role in modulating the convective systems over India. The instability and moisture are highest in
207 the coastal regions hence the frequency of severe thunderstorms and rainfall occurrences are comparatively
208 higher (Fig.4n,p). The North Western region shows the large values of thunderstorm frequency which is not
209 supported by other parameters. Hence, it may be inferred that this is due to frequent dry storms called "Andhi"
210 which have no relation with convective instability and rainfall (Rajpal and Deka, 1980). Thus, it can be
211 concluded that the effect of convection is large in the coastal regions compared to other regions which resulted
212 in high CAPE with more thunderstorms and intense rain occurrences.

3.3. Long-term trends in the instability parameters

214 The long-term trends are calculated for each parameter during the entire study period of 1980-2016 for all
215 regions using the robust regression analysis at 95% confidence interval as depicted in Fig. 5. For simplicity, the
216 average trends along with their standard deviation values are depicted in Table 1. Also to investigate about the
217 significance of trend values calculated from these time series datasets, a ttset analysis is done on all parameter
218 and locations. The p values are calculated at 95% confidence limits and they are depicted in Table 1. It is very
219 interesting to note that the p values are always lesser than 0.05; hence the time series variations to be presented
220 in subsequent sections will always be statistically significant in nature. The LCL (Fig.5a) height is found to
221 decrease which may lead to an overall increase in the number of rain occurrences throughout the country
222 (provided that the amount of atmospheric instability is adequate). On contrary, LFC (Fig.5b) is found to ascend
223 in all the regions resulting in the reduction of lower level instability and a strengthening of CINE (Fig.5h).
224 However, the extent of change in LFC (Fig.5b) and LCL (Fig.5a) is minimum in the coastal regions (~10 hPa).
225 In case of EL (Fig.5a), a drastic increase is depicted in all regions (highest in coastal regions) which increase the
226 height of the buoyant column; hence the net effect on total instability and CAPE (Fig.5f) is expected to increase
227 prominently. Similarly, LI (Fig.5d) values also show an enhancement in all the regions with slightly higher
228 magnitudes in the coastal regions. VT represents the lower level atmospheric instability and hence is expected to
229 be affected by the elevation in LFC. Thus, a reduction in VT (Fig.5e) is seen with minimum values in the coastal
230 regions (~0.3), medium in the NE and NW regions (~0.5) and highest in deep inland regions such as CI and PI
231 (~0.8). An intensification in CAPE (Fig.5f) is seen in all regions (~1100 J/kg) as expected from EL (Fig.5c) and
232 LI. However, the increase is the highest (~100%) at the coastal regions whereas in MLC (Fig.5g), which is
233 measured only up to 300 hPa level, the increment is only 20% of that in CAPE. Hence, it follows that the
234 maximum contribution towards the strengthening of CAPE comes above 300 hPa. In case of CINE, an overall
235 enhancement is observed as expected (~60 J/kg). In addition, the trend values suggest a two-fold increase of
236 CINE in inland regions while the values are much lesser (50%) in the coastal regions due to balancing effect
237 from strong convections and CAPE in those regions.

238   The PWV (Fig.5i) and PWL (Fig.5j) values are increasing similar to CAPE and MLC. The long-term

239   trends in PWV are about 10% of its climatological average with highest in the coastal regions. Further, the

240   lower level moisture content of PWL (up to 700 hPa) showed an increase but the trend values are comparatively

241   smaller (~6%). Hence, the mid and upper tropospheric moisture plays a crucial role in modulating the Indian

242   climate. The WSH (Fig.5k) parameter increases in all regions of the country, and hence it produces an inhibiting

243   effect on the lower level instability. An upper tropospheric cooling is found in all other regions (Fig. 5l) with

244   minimum values in the inland regions and maximum in the coastal regions. Consequently, the increase in CAPE

245   values is maximum in the coastal regions and lesser elsewhere. The ordinary thunderstorm frequency is also

246   found to increase (Fig. 5m) which may be due to the partial damping effect of an elevated LFC and CINE on

247   lower level instabilities. However, the TSS (Fig.5n) is found to increase drastically with a doubling effect in the

248   coastal regions. On the other hand, an increase in CINE and decrease of VT lead to an increase in the number of

249   WRF (Fig.5o). However, due to rise in CAPE and TSS (Fig.5n), the SRF (Fig.5p) is also found to rise

250   significantly by about 20% particularly in the coastal regions. It may be noted that, as EL has more dominant

251   effect on CAPE hence the rise in SRF is much larger than that WRF (5%). Finally, the long-term trends have

252   been compared between the east and west coastal regions and it is observed that the rate of increase in total

253   instability is the most prominent in the western coasts while factors related to ascending LFC, CINE and

254   reducing VT are more significant in the central India which is the farthest from both the sea coasts. Thus, the

255   long-term analysis infers that lower atmospheric instability has reduced while the upper tropospheric instability

256   and moisture increased drastically over the Indian region. As a result, convective severity as expressed in terms

257   of CAPE, TSS and SRF is increasing more strongly in the coastal regions while in the continental areas this

258   effect is dampened due to the contribution of increasing CINE and WSH.

259   3.4. Seasonal effect on long-term trends in the instability parameters

260   The seasonal variation of atmospheric instability is shown in Fig. 6. LCL shows a uniform descent by

261   10 hPa in all seasons (Fig.6a) whereas LFC ascends in most of the regions and seasons (Fig.6b). However, this

262   ascent is more prominent in the monsoon and post-monsoon due to the occurrence of more convective rain. The

263   seasonal variation is absent in EL and LI (Fig.6c,d) which are mainly associated with an upper layer

264   phenomenon. VT shows the most prominent weakening in monsoon and post-monsoon seasons (Fig.6e). MLC

265   and CAPE show a lot of regional disparities with a uniform increase in its value in all the seasons (Fig.6f,g). In

266   monsoon and post-monsoon, the increase in CAPE is slightly lesser due to the effect of decreasing VT and

267   elevated LFC. CINE is closely related to VT and LFC, hence it shows slight strengthening in the monsoon and

268   post-monsoon seasons with maximum values in inland regions as expected (Fig.6h).

269   PWV, PWL and WSH represent a prominent increase in the monsoon followed by the post-monsoon

270   (Fig.6i-k). T100 is related to an upper atmospheric phenomenon hence no seasonal or spatial variation is

271   displayed, except for a small strengthening in pre-monsoon (Fig.6l) due to the prevalence of intense convections

272   events which is supported by the strongest increase in CAPE. A decrease in lower atmospheric instability and

273   increase in CINE is observed; hence TSO and WRF are expected to increase. However, this increase is found

274   more dominant only in the monsoon and post-monsoon (Fig.6m,o). Another interesting result is that TSS and

275   SRF donot behave similarly. TSS increases almost uniformly in all seasons with the highest in the pre-monsoon.

276   However, SRF increases mainly in the monsoon followed by the post-monsoon season (Fig.6n,p). The observed

disparity between them is due to the profuse moisture availability during monsoon and post-monsoon compared to the pre-monsoon.

Further, in seasonal trends, east and west coasts show equivalent trends in all instability parameters while the Central India still remains as the region which is most affected by the ascension of LFC and CINE. Thus, the seasonal analysis reveals that the yearly long-term trends are almost uniformly distributed in all the seasons. The ordinary and weak thunderstorm frequencies show the strongest increase during monsoon and post-monsoon while the upper atmospheric instability shows a weak influence in the pre-monsoonal trends on the yearly climatology.

3.5. Effect of specific periodicities on long-term trends

In case of both annual and seasonal trend analysis, all Indian sub-divisions are found to follow similar behavior. Hence, to find out the periodicities in the average long-term trends, the time series of all regions are averaged and then subjected to EMD technique which reveals the existence of four main periodicities namely: 1.5 - 2.5 years corresponding to QBO, 4-6 years corresponding to ENSO, 10-12 years corresponding to the solar cycle and the fourth one is of 16-20 years. A similar multi-decadal climatic oscillation was also reported by Dhaka et al. (2010). Hence for simplicity, this periodicity has been renamed as a Multi-decadal Climatic Oscillation (MCO).

The climatic trends of these periodicities for each parameter are calculated from robust regression analysis. An illustration of the obtained MCO periodicities for CAPE along all the Indian regions is shown in Fig. S2. Further for comparison, the trend values from each periodicity is normalized to percentage with respect to the total trend values for each parameters and the net contribution of these individual periodicities are depicted in Fig. 7. Fig. 7 suggests that ENSO, QBO and solar cycle have no effect on LCL (Fig.7a) while MCO is quite strong. LFC shows minimal effects to all periodicities except solar cycle period which may be due to solar-terrestrial heating (Fig.7b). EL and LI are significantly affected by both solar and MCO periodicities (Fig.7c-d). But in LI, the contribution from MCO is much more than solar effect. In case of VT (Fig. 7e) the effect of both ENSO and MCO are found prominent. CAPE is found to be strongly influenced by MCO followed by solar effect (Fig.7f) and this is also discernible from the most strong increasing trends in CAPE especially in the coastal regions after the years 1996-2000 in Fig. S2. However, in case of MLC, contribution of MCO is comparatively lesser (Fig.7g) hence some separate phenomena above 300 hPa may have prominent influence on increasing CAPE. Apart from CAPE, effect of MCO is also found very strong in case of CINE (Fig.7h).

The moisture parameters like PWV and PWL show similar variability as in CAPE and MLC which indicates significant moisture transport changes only above 300 hPa in the past 18 years (Fig.7i-j). WSH does not show the dominance of any periodicity (Fig.7k) while T100 shows the most prominent contribution from the MCO (Fig.7l) thereby showing its connection with the long-term variability in EL and CAPE with associated thunderstorm severity in the recent years. TSO and TSS are both affected by solar and MCO (Fig.7m-n) but TSS shows that the effect of MCO is higher compared to TSO. Finally, the effect of MCO is also found more prominent in case of SRF and WRF (Fig.7o-p). In nutshell, the MCO acts as the most dominant periodicity which has influenced the convective severity over India.

3.6. Investigation of two-part trends

In the previous section, the annual averaged time series of instability parameters showed a drastic change with respect to MCO. It has also been indicated from Fig. S2 that the climatic trends before and after the period 1996-2000 are significantly different from each other. Therefore, we have estimated the trends with respect to two segments before and after the year 1998. The time series for both MCO are produced and their trend values are represented in Fig. 8. For simplicity, the MCO are referred as C1 (1980 to 1998) and C2 (1999 to 2016), respectively. Starting with LCL, in C1 there is almost no change, but in C2 there is a strong descent which influences the overall change in the time series (Fig.8a). In case of LFC, C1 shows a decreasing trend, but in C2, a significant increasing pattern is seen hence an overall increase is observed in LFC (Fig.8b). An increase in EL is noticed in both the periods however during C2 the trends show significant enhancement (Fig.8c). LI is expected to strengthen from 37 years trend, however it shows a slight weakening in C1 followed by a prominent strengthening in C2 resulting in a net increasing trend (Fig.8d). VT shows an overall decreasing pattern in both the periods (Fig.8e). CAPE (Fig.8f) shows an enhancement in both the cycles but the trends become more prominent in C2 (1500 J/Kg). Similar to CAPE, MLC (Fig.8g) also shows an increasing trend in both the cycles but the trend values are also much smaller than in CAPE. Hence, the rise in EL height can be considered as a primary factor for the increase in CAPE above 300 hPa during C2. CINE shows increasing trend in both C1 and C2 but again the trend values are much stronger (~80 J/kg) during C2 especially in the inland regions (Fig.8h).

The moisture trends in both PWV and PWL have shown a constant increase in both the MCO throughout India (Fig.8i-j). The WSH (Fig.8k) also increases uniformly in both MCO with strongest trends in the inland regions. A prominent cooling of ~1.5 degrees is seen in 100 hPa levels everywhere in C1, but in C2 the trend increases to ~2.5 degrees (Fig.8l) which can be considered responsible for the abrupt elevation in EL and strengthening in CAPE values during the recent years. TSO increases slightly in C2 compared to C1 (Fig.8m). But in case of TSS, the positive trend gets doubled in C2 mainly in the coastal regions (Fig.8n). Finally, in case of SRF the trend values in C2 are slightly higher with the maximum magnitudes in the coastal regions as expected (Fig.8p). A further comparison between the six regions reveals that the west coast shows the maximum enhancement in all the instability and convective severity parameters in the past 18 years due to strong growth in moisture content and associated cooling at 100 hPa.

On the contrary, during C2 central India suffers from the maximum reduction in lower level instability as seen in CINE and LFC due to the dearth of moisture content. Similar results are also found in other coastal and inland regions. Hence it follows that mainly during C2, the upper tropospheric instability has enhanced everywhere while the lower tropospheric instability has weakened which has led to the development in both CAPE and CINE. As a result both TSS-TSO and WRF -SRF combination increases.

4. Discussion

From the previous section, it is inferred that a cooling trend at 100 hPa levels has led to the ascent in EL which results in an increase in CAPE, TSS and SRF. To explain the reason behind this, we consider the ozone to be a primary heating agent by absorbing the incoming solar ultraviolet radiation near 100 hPa level (Mohankumar, 2008). OH hydroxyl radicals are formed by oxidation of water vapor molecules by a reactive oxygen atom at the same height. On the other hand, it has been reported by Forster et al. (2007) that in the recent years there has been a cooling in upper troposphere due to ozone breakup near 70 hPa. Hence, it is hypothesized

357   that the OH radicals formed from the oxidation of water vapour can take an active role in the breakup of ozone

358   molecules at 100 hPa levels which may lead to this cooling effect. The preceding sections have shown a

359   significant increase in moisture content especially in the coastal areas hinting towards more moisture transport

360   from the adjoining seas. Again, an increase in LI and CAPE values have also been reported in most of the

361   regions which can lift the available moisture to upper atmospheric levels (Das et al., 2016; Guha et al., 2017).

362   To add to this increasing CAPE and LI, many recent researchers' have reported a net increase in the Hadley cell

363   and Brewer-Dobson circulation strength (Liu et al., 2012; Lu et al., 2007; Fu et al., 2015; Shepherd and

364   McLandress, 2011) which also assists in the up-liftment of moisture to upper atmospheric levels. Thus, it is

365   inferred that low-level moisture is transported to the upper troposphere and above where it is responsible for

366   ozone depletion and cooling thereby elevating the EL and increasing the thunderstorm severity.

367   To test this hypothesis, yearly averaged time series of specific humidity and ozone mixing ratio data are

368   collected for all stations and the two-part trend values are depicted in Fig. 9. This figure shows a rise in specific

369   humidity levels by 7% in C2 over entire India (Fig.9a). On the other hand, trends of specific humidity have

370   almost trebled in C2 phase with the maximum values in the coastal regions (Fig.9e). As water vapor

371   concentration increases, ozone concentration is expected to decrease. The ozone trends support this hypothesis

372   by showing a sharp transition from low positive to high negative values during C2 (Fig.9b,f). It may be

373   additionally noted that the specific humidity increase and reduction in ozone content are strongest in the coastal

374   regions leading to a higher increase in CAPE and severe thunderstorms in those regions.

375   In the recent decades, Indian region has experienced a surface warming trend which is mainly caused

376   by a dominant increase in greenhouse gas concentrations as pointed out by Basha et al.   (2017). These

377   greenhouse gases are heat absorbing in nature and these particles reside within the lower troposphere (generally

378   below 700 hPa) due to surface heating and boundary layer dynamics as reported by Chakraborty et al. (2017b).

379   Further, these gases has a tendency to absorb and then re-emit the outgoing longwave radiation as emitted by the

380   earth resulting more downward longwave radiation flux and atmospheric heating which elevates the LFC.

381   Additionally, this near surface heating reduces the vertical temperature lapse rate leading to weakening the

382   lower instability (VT). To prove this hypothesis, yearly averaged DLWRF time series is depicted over Indian

383   region in Fig. 9(c,g) which also suggests that DLWRF values are increasing prominently in C2. To show that

384   the increase in DLWRF is due to the heat absorbing particles only, the trends in Absorbing Aerosol Index (AAI)

385   are shown for all the regions. The figure suggests that the mean of AAI is increasing sharply in C2 with a

386   positive trend (Fig.9d,h). Due to this heating of lower atmosphere and capping of lapse rates by greenhouse

387   gases and absorptive aerosols, the LFC starts ascending, so WSH and CINE get stronger while VT reduces. As a

388   result the ordinary to weak convective occurrences start increasing.

389   Finally, it has to be explained why the upper air instability and CAPE are increasing mainly in the

390   coastal regions. The coastal regions have high moisture content (Saha et al., 2017). Because of the strong land-

391   ocean contrast, low-level winds close to 850 hPa flow into the coastal regions and disperse the pollutants and

392   greenhouse gases to other locations leading to a weaker convective inhibition in those areas. This hypothesis is

393   supported by the lowest AAI values in the coasts despite having high increasing trends in those areas. In

394   addition, the ample moisture supply in the coastal regions is lifted up to the upper troposphere and lower

395   stratosphere (UTLS) where it undergoes strong cooling due to ozone decomposition. Hence, the EL ascends

396   more resulting in higher CAPE which finally led to an abrupt rise in TSS and SRF in the coastal regions.

397   However, in the inland regions the layer of absorptive aerosols and greenhouse gases cannot be dispersed amply
398   due to the dearth of transported moisture at the lower levels. As a result, the lower atmospheric instability gets
399   limited in inland regions. Further, due to less moisture availability, UTLS cooling and EL ascent are much lower
400   hence there is a less rise in CAPE which ultimately leads to an increase in TSO and WRF in those sub-divisions.
401   It may be noted that the trend in AAI are not significantly different in the two halves of the analysis. Again, it is
402   the EL and not the LFC or LCL which influences CAPE strongly; hence the strong trends of humidity increase
403   and ozone reduction overpowers the weaker inhibitory effect from the atmospheric aerosols and this acts as a
404   major driving force behind the increase in convective severity compared to in most of the cases.

405

406   **5. Summary and conclusions**

407   In recent decades, global warming has become a threat to human life and society in terms of its various
408   implications. Increase in surface temperature leads to stronger atmospheric instabilities which in term may
409   increase the CAPE resulting in more severe thunderstorm and precipitation activity. Hence, the long term
410   variations of instability parameters will help to better understand the changes in the weather extremes with
411   respect to climate change. In light of the above, the main objective of the present study is to check whether
412   convective instability is changing over the Indian region during the last 37 years, and then to find its possible
413   effects on thunderstorm and rainfall severity. Radiosonde measurements from Integrated Global Radiosonde
414   Archives (IGRA) pertaining to 27 stations across 6 Indian sub-divisions are utilized to depict the spatial
415   distribution of these long-term trends. The selection of instability parameters is done based on Principle
416   Component Test (PCT) which showed the importance of taking LI and VT for further investigations. A total of
417   16 parameters (including parcel and instability data with moisture content, wind shear, and thunderstorm and
418   rainfall frequencies) have been utilized. Robust fit approach is employed on the regional average time series to
419   calculate the long-term trends on both yearly and seasonal basis. The main highlights obtained from the present
420   study are listed below:

421   1. The coastal regions experience a significant increase in Convective Available Potential Energy (CAPE)
422   and Equilibrium Level (EL) leading to more occurrences of Severe Thunderstorms (TSS) and severe
423   rainfall events (SRF) while the inland regions suffer from a decrease in lower atmospheric instability due
424   to elevated Convective Inhibition Energy (CINE) and Level of Free Convection resulting in more Ordinary
425   thunderstorm (TSO) and Weak Rainfall occurrences (WRF).

426   2. Seasonal variation of LFC, CINE, Wind Shear (WSH), TSO and WRF shows drastic increase during
427   monsoon and post-monsoon seasons while strengthening in CAPE, EL, Lifted Index (LI) and TSS are
428   found more prominent during the pre-monsoon.

429   3. The Empirical Mode Decomposition (EMD) analysis on the instability parameters reveals that the 16-20
430   year multi-decadal oscillation (MCO) as the most dominant component in all six Indian sub-divisions.

431   4. The two-part analysis reveals that many parameters like EL, CAPE, CINE, Temperature at 100 hPa
432   (T100), TSO and TSS show significant rise during C2 (1999-2016) which dominates 37-year trend.

433   5. The annual and two-part trends support that the increase in thunderstorm severity and associated
434   convection is strongest along western coasts due to maximum moisture ingress while the greatest reduction
435   in lower atmospheric instability is experienced in central India owing to its largest distance from the seas.

6. In the coastal regions, ample amount of water vapor is advected into the mid-troposphere from the surrounding seas which in presence of strong lifting goes up to upper troposphere and lower stratosphere (UTLS) where it decomposes to OH radical and further breaks down the ozone particles leading to a strong cooling effect. This cooling effect will ascend the EL resulting in much stronger LI and CAPE, hence more TSS and SRF.

7. In the inland regions, the dispersing effect by sea winds is absent hence the capping effect of lower instability is more leading to stronger CINE values. Again, due to the dearth of moisture transport from the seas, the UTLS cooling is lesser; leading to a weaker rise in CAPE consequently the TSO and WRF frequencies increase significantly.

8. However, as EL has a stronger contribution over increasing CAPE than the inhibitory effect of LFC, hence the long term trends are expected to be more strongly influenced by the ozone decomposition and cooling at 100 hPa levels than the capping effect of low level inversions from absorptive aerosols; hence the convective severity over the Indian regions is found to increase.

Thus, it may be inferred that in the near future also, convective severity will increase strongly in the coastal regions while weak and ordinary thunderstorms will be more common in the inland regions. It may also be noted that this study supports and explains the hypothesis brought forward by early research attempts that UTLS cooling at 100 hPa and greenhouse gases concentration rise can regulate the climatic trends of convective severity and frequency. However, this set of explanations is based on isolated information from selected in-situ observations and hence it needs to be studied in more detail spatially in future using model-based observations. In the recent years, certain studies have utilized multiple GCM outputs over the US to infer the robust increase in thunderstorm frequency (Diffenbaugh et al., 2013; Seeley and Romps, 2015). However, these types of studies have not yet been done over the Indian region. Hence, a combination of multi-station radiosonde data with model data will be utilized to provide a generalized picture about convective severity over Indian region.

Acknowledgments

One of the authors (Rohit Chakraborty) thanks, Science and Engineering Research Board, Department of Science and Technology for providing fellowship under National Post-Doctoral Scheme (File No:PDF/2016/001939). He also acknowledges National Atmospheric Research Laboratory, for providing necessary support and data for this work. The authors also thank S.T. Akhil Raj, Sanjeev Dwivedi and N. Narendra Reddy for their suggestions. Data used in present study can be obtained directly from IGRA website.

References

Alappattu, D.P. and Kunhikrishnan, P.K.: Premonsoon estimates of convective available potential energy over oceanic region surrounding Indian subcontinent. J. Geophys. Res..Atmos. 114, 2009.

Ananthakrishnan, R.: Some aspects of the monsoon circulation and monsoon rainfall. Pure Appl. Geophys., 115(5–6), 1209–1249, 1977.

Andersen, R.: Modern methods for robust regression. Sage, 2008.

Basha, G., Kishore, P., Ratnam, M. V., Jayaraman, A., Kouchak, A. A., Ouarda, T. B. M. J., and Velicogna, I.: Historical and Projected Surface Temperature over India during 20 th and 21 st century. Sci. Rep., 7(1), 2987, 2017.

476   Brooks, H. E.: Severe thunderstorms and climate change. Atmos. Res., 123, 129–138, 2013.

477   Chakraborty, R. and Maitra, A.: Retrieval of atmospheric properties with radiometric measurements using
478   neural network. Atmos. Res., 181:124–132, https://doi.org/10.1016/j.atmosres.2016.05.011,2016.

479   Chakraborty, R., Talukdar, S., Saha, U., Jana, S., and Maitra, A.: Anomalies in relative humidity profile in the
480   boundary layer during convective rain. Atmos. Res., 191, https://doi.org/10.1016/j.atmosres.2017.03.011,
481   2017a. Chakraborty, R., Saha, U., Singh, A. K., and Maitra, A.: Association of atmospheric pollution and
482   instability indices: A detailed investigation over an Indian urban metropolis. Atmos. Res.,
483   https://doi.org/10.1016/j.atmosres.2017.04.033, 2017b.

484   Chakraborty, R., Basha, G., Ratnam and M.V.: Diurnal and long-term variation of instability indices over a
485   tropical region in India. Atmos. Res., https://doi.org/10.1016/j.atmosres.2018.03.012, 2018.

486   Das, S.S., Ratnam, M.V., Uma, K.N., Patra, A.K., Subrahmanyam, K.V., Girach, I.A., Suneeth, K.V., Kumar
487   K.K., and Ramkumar, G.: Stratospheric intrusion in to the troposphere during the tropical cyclone Nilam
488   (2012), Q. J. R. Meteorolog. Soc. doi: 10.1002/qj.2810, 2016.

489   Dhaka, S. K., Sapra, R., Panwar, V., Goel, A., Bhatnagar, R., Kaur, M.,: Influence of large-scale variations in
490   convective available potential energy (CAPE) and solar cycle over temperature in the tropopause region at
491   Delhi (28.3oN, 77.1oE), Kolkata (22.3o N, 88.2o E), Cochin (10o N, 77o E), and Trivandrum (8.5oN,
492   77.0oE) using radiosonde during 1980--2005. Earth Planets Space, 62(3), 319–331, 2010.

493   Diffenbaugh, N. S., Scherer, M., and Trapp, R. J.: Robust increases in severe thunderstorm environments in
494   response to greenhouse forcing. Proc. Natl. Acad. Sci., 110(41), 16361–16366, 2013.

495   Durre, I., Vose, R. S., and Wuertz, D. B.: Overview of integrated global radiosonde archive. J. Clim., 19(1), 53–
496   68, 2006.

497   Emanuel, K.: Climate and tropical cyclone activity: A new model downscaling approach. J. Clim., 19(19),
498   4797–4802, 2006.

499   Forster, P. M., Bodeker, G., Schofield, R., Solomon, S. and D. Thompson: Effects of ozone cooling in the
500   tropical lower stratosphere and upper troposphere, Geophys. Res. Lett., 34, L23813,
501   doi:10.1029/2007GL031994, 2007.

502   Fu, Q., Lin, P., Solomon, S., and Hartmann, D. L.: Observational evidence of thestrengthening of the Brewer-
503   Dobson circulation since 1980. J. Geophys. Res. Atmos., 120(19), 2015.

504   Gensini, V. A., and Mote, T. L.: Downscaled estimates of late 21st century severe weather from CCSM3. Clim.
505   Change, 129 (1-2), 307-321, 2015.

506   Gettelman, A., Seidel, D. J., Wheeler, M. C., and Ross, R. J.: Multidecadal trends in tropical convective
507   available potential energy. J. Geophys. Res. Atmos. 107(D21), 2002.

508   Huntrieser , H., Schiesser, H.H., Schmid, W.,and Waldvogel, A.: Comparison of traditional and Newly
509   Developed Thunderstorm Indices for Switzerland, Weather Forecasting, 12, 108-125, 1997.

510   De Graaf, M., Stammes, P., Torres, O., and Koelemeijer, R. B. A.: Absorbing Aerosol Index: Sensitivity
511   analysis, application to GOME and comparison with TOMS. J. Geophys. Res. Atmos., 110(D1), 2005.

512   Guha, B. K., Chakraborty, R., Saha, U., and Maitra, A.: Tropopause height characteristics associated with ozone
513   and stratospheric moistening during intense convective activity over Indian sub-continent. Global Planet.
514   Change, 158. https://doi.org/10.1016/j.gloplacha.2017.09.009, 2017.

515 Joseph, P. V., Raipal, D. K., and Deka, S. N.: Andhi. The Convective Dust Storms of Northwest India. Mausam,
516   31, 431–442, 1980.

517 Karmakar, S.: Climatology of thunderstorm days over Bangladesh during the pre-monsoon season. J Bangladesh
518   Acad. Sci, 3(1), 103–112, 2001.

519 Kharin, V. V, Zwiers, F. W., Zhang, X., and Wehner, M.: Changes in temperature and precipitation extremes in
520   the CMIP5 ensemble. Clim. Change, 119(2), 345–357, 2013.

521 Liu, J., Song, M., Hu, Y., and Ren, X.: Changes in the strength and width of the Hadley circulation since 1871.
522   The climate of the Past, 8(4), 1169–1175, 2012.

523 Lu, J., Vecchi, G. A., Reichler.: Expansion of Hadley cell by global warming. Geophys. Res. Lett., 34(6), 2007.

524 Manohar, G. K., Kandalgaonkar, S. S., and Tinmaker, M. I. R: Thunderstorm activity India and Indian
525   southwest monsoon. J. Geophys. Res. Atmos. 104(D4), 4169–4188, 1999.

526 Mohanakumar, K.:Stratosphere-troposphere interactions: introduction.Springer Science Business Media, 2008.

527 Murthy, B.S. and Sivaramakrishnan, S.: Moist convective instability over the Arabian Sea during the Asian
528   summer monsoon, 2002, Meteorol. Appl., https://doi.org/10.1017/S135048270500201X, 2006.

529 Murugavel, P., Pawar, S. D., and Gopalakrishnan, V.: Trends of convective available potential energy over the
530   Indian region and its effect on rainfall. Int. J. Climatol., 32(9), 1362–1372, 2012.

531 Nelli, N. R., Ratnam, M.V., Basha, G., and Ravikiran, V.: Cloud vertical structure over a tropical station
532   obtained using long-term high resolution Radiosonde measurements, Atmos. Chem. Phys. Discuss.,
533   https://doi.org/10.5194/acp-2018-194, 2018.

534 Nelli, N. R., and Rao, K.G..: Contrasting variations in the surface layer structure between the convective and
535   non-convective periods in the summer monsoon season for Bangalore location during PRWONAM, J.
536   Atmos. Sol. Terr. Phys., https://doi.org/10.1016/j.jastp.2017.11.017, 2018.

537 Pai, D. S., Sridhar, L., Rajeevan, M., Sreejith, O. P., Satbhai, N. S., and Mukhopadhyay, B.: Development of a
538   new high spatial resolution (0.25$\times$ 0.25) long period (1901--2010) daily gridded rainfall data set over
539   India and its comparison with existing data sets over the region. Mausam, 65(1), 1–18, 2014.

540 Prein, A. F., Rasmussen, R. M., Ikeda, K., Liu, C., Clark, M. P., and Holland, G. J.: The future intensification of
541   hourly precipitation extremes. Nat. Clim. Change, 7(1), 48, 2017.

542 Raj, S. T. A., Ratnam, M. V., Rao, D. N., and Murthy, B. V. K.: Long-term trends in stratospheric ozone,
543   temperature, and water vapor over the Indian region. Ann. Geophys. (Vol. 36, p. 149), 2018.

544 Rajeevan, M., Bhate, J., Kale, J. D., and Lal, B.: High resolution daily gridded rainfall data for the Indian
545   region: Analysis of break and active monsoon spells. Current Science, 296–306, 2006.

546 Rajeevan, M., Bhate, J., and Jaswal, A. K.: Analysis of variability and trends of extreme rainfall events over
547   India using 104 years of gridded daily rainfall data. Geophys. Res. Lett., 35(18), 2008.

548 Raipal, D. K., and Deka, S. N: ANDHI, convective dust storm of northwest India. Mausam, 31, 431–442, 1980.

549 Rao, Y. P.:Southwest monsoon. Synoptic Meteorology, 1976.

550 Riemann-Campe, K., Fraedrich, K., and Lunkeit, F.: A global climatology of convective available potential
551   energy (CAPE) and convective inhibition (CIN) in ERA-40 reanalysis. Atmos. Res., 93(1), 534–545, 2009.

552 Saha, U., Maitra, A., Midya, S. K., and Das, G. K.: Association of thunderstorm frequency with rainfall
553   occurrences over an Indian urban metropolis. Atmos. Res., 138, 240–252, 2014.

554 Saha, U., Chakraborty, R., Maitra, A., and Singh, A. K.: East-west coastal asymmetry in the summertime near-
555   surface wind speed and its projected change in future climate over the Indian region. Glob. Planet. Change,
556   152., https://doi.org/10.1016/j.gloplacha.2017.03.001, 2017.

557 Santhi, Y. D., Ratnam, M. V., Dhaka, S. K., and Rao, S. V.: Global morphology of convection indices observed
558   using COSMIC GPS RO satellite measurements. Atmos. Res., 137, 205–215, 2014.

559 Seeley, J. T., and Romps, D. M.: The effect of global warming on severe thunderstorms in the United States. J.
560   Clim., 28(6), 2443–2458, 2015.

561 Shepard, D.: A two-dimensional interpolation function for irregularly-spaced data. In Proceedings of the 1968
562   23rd ACM national conference (pp. 517–524), 1968.

563 Shepherd, T. G., and McLandress, C.: A robust mechanism for thestrengthening of the Brewer-Dobson
564   circulation in response to climate change: Critical-layer control of subtropical wave breaking. J. Atmos. Sci.,
565   68(4), 784–797, 2011.

566 Trenberth, K. E., Dai, A., Rasmussen, R. M., and Parsons, D. B.: The changing character of precipitation. Bull.
567   Am. Meteorol. Soc., 84(9), 1205–1217, 2003.

568 Wang, S.-Y., Davies, R. E., Huang, W.-R., and Gillies, R. R.: Pakistan's two-stage monsoon and links with the
569   recent climate change. J. Geophys. Res. Atmos., 116(D16), 2011.

570 Webster, P. J., Holland, G. J., Curry, J. A., and Chang, H.-R.: Changes in tropical cyclone number, duration, and
571   intensity in a warming environment. Science, 309(5742), 1844–1846, 2005.

572 Wu, Z., and Huang, N. E.: Ensemble empirical mode decomposition: a noise-assisted data analysis method.
573   Advances in Adaptive Data Analysis, 1(1), 1–41, 2009.

574 Xie, B., Zhang, Q., and Ying, Y.: Trends in precipitable water and relative humidity in China: 1979--2005. J.
575   Appl. Meteorol. Clim., 50(10), 1985–1994,2011.

576

577

578

Name	CI			EC			NE			NW			PI			WC			India		
	μ	σ	p	μ	σ	p	μ	σ	p	μ	σ	p	μ	σ	p	μ	σ	p	μ	σ	p
LCL	39	2.8	1.7E-7	8.9	0.1	3.0E-8	15.4	0	1.5E-6	24	0.6	1.8E-9	45.5	1.0	1.2E-7	9.1	0.2	1.0E-8	23	6.4	7.7E-9
LFC	-38	1.4	7.8E-7	-11	0.2	2.1E-6	13.4	0.1	3.6E-6	-44	3.8	8.2E-7	-9.2	0.0	2.4E-6	-17	0.6	8.8E-6	-18	8.7	5.7E-7
EL	-188	11.2	4.3E-9	-280	27.1	2.0E-6	-206	8.8	2.6E-8	-230	2.0	2.7E-8	-239	6	4.3E-7	-311	40	9.5E-6	-242	19	4.1E-9
LI	-0.8	0.01	4.9E-7	-1.7	0.2	3.2E-8	-1.3	0.1	6.2E-8	-1.1	0.1	3.4E-6	-1.4	0.0	6.4E-9	-1.8	0.1	2.4E-8	-1.3	0.1	6.5E-9
VT	-0.7	0.01	3.2E-9	-0.3	0.02	1.3E-9	-0.5	0	1.5E-7	-0.5	0.0	1.3E-9	-0.9	0.1	3.2E-8	-0.4	0.0	1.1E-9	-0.5	0.1	8.2E-8
CAPE	617	2.9	1.2E-5	1589	90.8	3.3E-6	1137	30	6.5E-6	858	53	2.8E-5	1000	39	2.7E-6	1554	198	1.9E-6	1126	159	3.3E-6
MLC	55	0.24	2.7E-8	288	9.6	1.7E-8	273	4.8	1.8E-8	134	1.1	1.2E-7	201	16	9.9E-9	323	27	3.4E-8	212	42	5.6E-9
CINE	-94	7.4	3.0E-4	-36	0.3	4.1E-5	-30	1.2	1.0E-4	-85	6.9	5.1E-5	-67	2.4	1.6E-3	-44	1.5	9.4E-4	-59	11	9.2E-5
PWV	1.4	0.03	1.9E-9	3.2	0.03	2.2E-9	3.7	0.1	3.3E-9	1.3	0.0	3.8E-8	2.2	0.0	2.6E-9	3.9	0.1	8.1E-9	2.6	0.5	8.2E-9
PWL	-0.2	0	6.6E-8	0.4	0	2.7E-9	0.7	0.1	5.8E-8	0.0	0	6.6E-9	0.6	0.0	3.6E-9	0.6	0.0	5.8E-9	0.4	0.2	1.8E-9
WSH	5.8	0.3	3.0E-3	3.4	0.2	9.7E-3	4.8	0.2	2.0E-4	3.4	0.0	6.2E-5	5.5	0.6	4.4E-4	3.6	0.1	5.6E-3	4.4	0.4	2.5E-3
T100	-1.5	0.03	9.2E-8	-2.5	0.1	1.5E-8	-0.4	0	3.6E-8	-0.3	0	2.4E-9	-2.5	0.3	2.4E-8	-2.2	0.2	2.0E-7	-1.6	0.4	1.2E-9
TSO	1.4	0.05	4.0E-4	0.8	0	2.4E-6	2.2	0.0	5.0E-4	3.5	0.2	5.0E-4	2.7	0.2	1.9E-4	0.5	0	1.2E-5	1.8	0.5	4.5E-5
TSS	1.5	0.0	2.0E-4	2.3	0.05	1.8E-6	2	0.1	2.0E-4	2.5	0.3	5.1E-5	1.7	0.1	1.9E-4	2.3	0.1	8.8E-6	2.1	0.2	1.2E-5
WRF	2.9	0.1	4.0E-3	3.8	0.1	5.3E-5	4.6	0.4	2.0E-3	2.2	0.0	3.0E-3	2.8	0.1	9.0E-4	6.3	0.2	9.7E-5	3.8	0.6	3.5E-4
SRF	0.4	0.0	3.0E-7	0.8	0.06	5.0E-5	0.2	0.0	1.3E-5	0.2	0	1.3E-3	0.2	0	9.7E-7	1.1	0.1	2.8E-7	0.5	0.2	2.2E-4

579 **Table 1: Statistical Information related to the 37-year trend of all instability parameters over the six sub-divisions of India.**

Figures
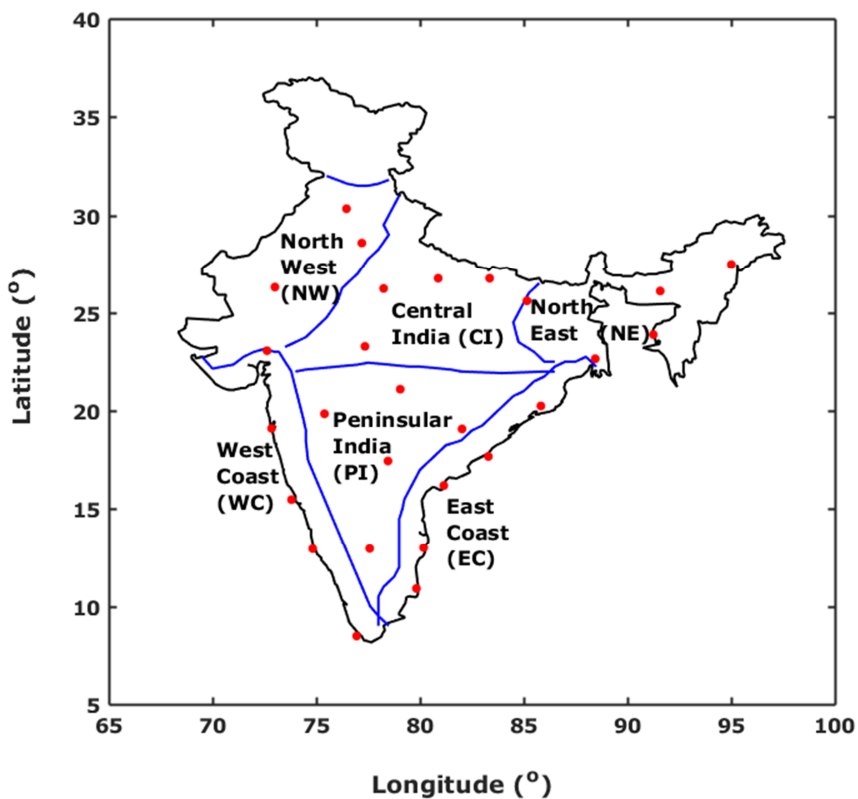
Figure 1: The locations of the 27 IGRA stations used for the present study. The distribution of the 27 stations over Indian regions is as follows: 4 stations in the NC, 6 stations in EC, 4 stations in NE, 4 stations in the NW, 5 stations in the PI and finally 4 stations in WC.
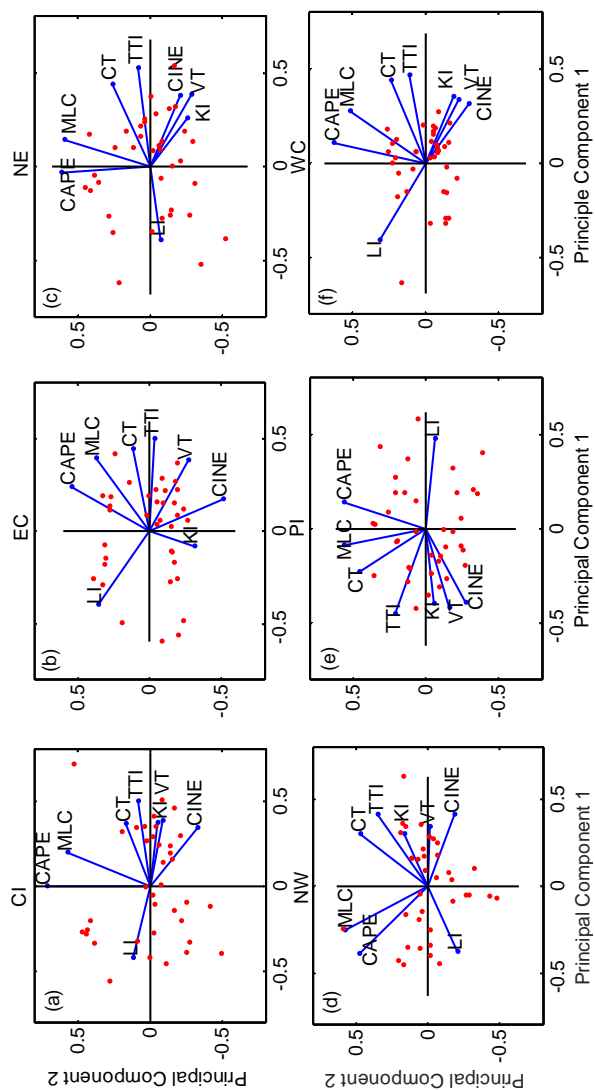
Figure 2: Principle Component Analysis for selection of instability parameters for the long-term trend study in (a) Central India, (b) East Coast, (c), North East, (d) North West, (e) Peninsular India and (f) West Coasts obtained using IGRA observations.
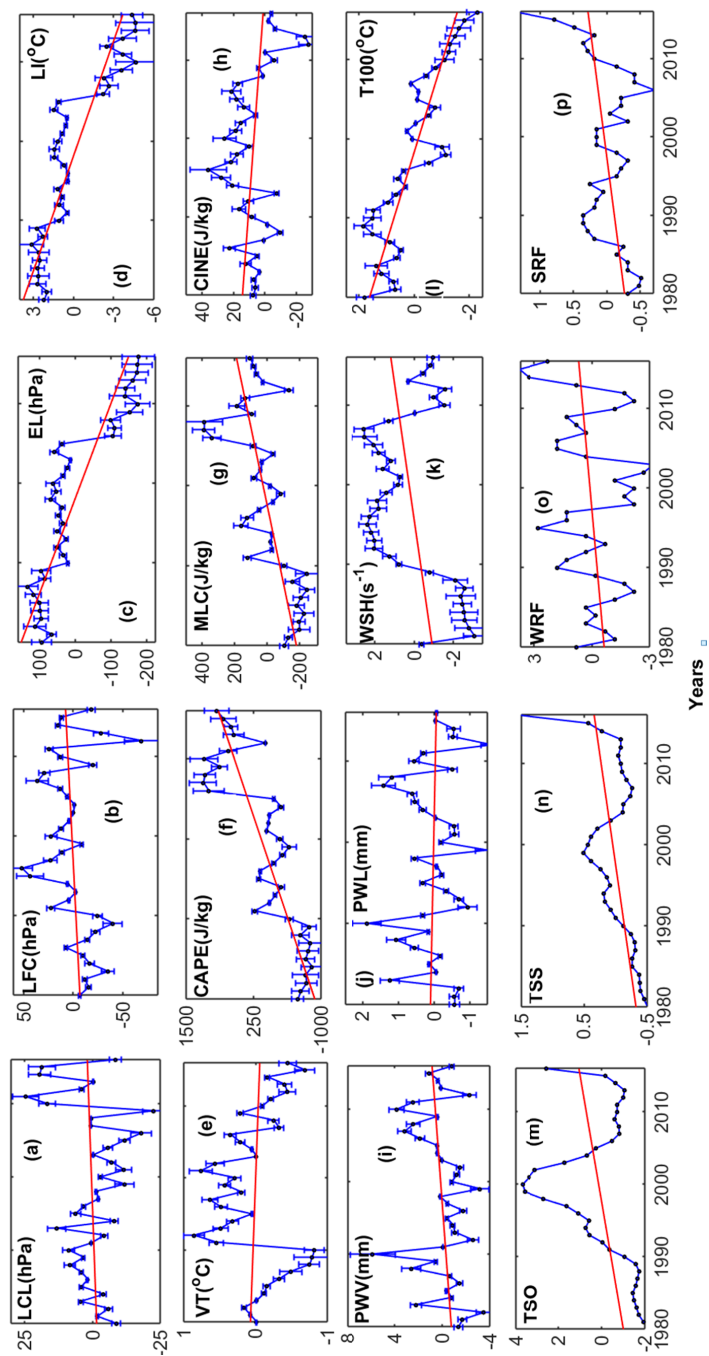
Figure 3: Long-term variation of (a) LCL, (b) LFC, (c) EL, (d) LI, (e) VT, (f) CAPE, (g) MLC, (h) CINE, (i) PWV, (j) PWL, (k) WSH, (l) T100, (m) TSO, (n) TSS, (o) WRF and (p) SRF observed over Chennai.
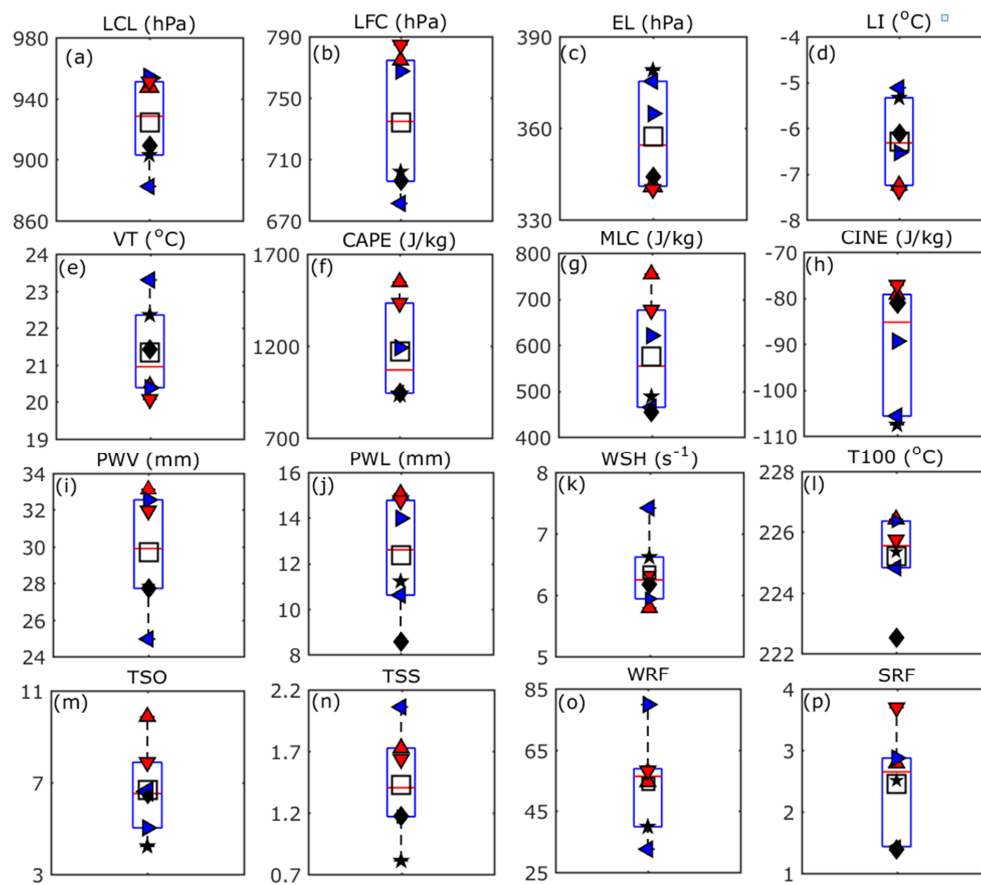
Figure 4: Climatological mean values of (a) LCL, (b) LFC, (c) EL, (d) LI, (e) VT, (f) CAPE, (g) MLC, (h) CINE, (i) PWV, (j) PWL, (k) WSH, (l) T100, (m) TSO, (n) TSS, (o) WRF and (p) SRF over the six subdivisions of India. Coastal Regions are represented by red cones, the north eastern and western regions are denoted by black stars and diamonds while the blue cones represent the inland regions. Here the box limits refer to the upper and lower quartiles (25% and 75%) while the whiskers refer to the outlier limit of the data (5% and 95% limit of the population)
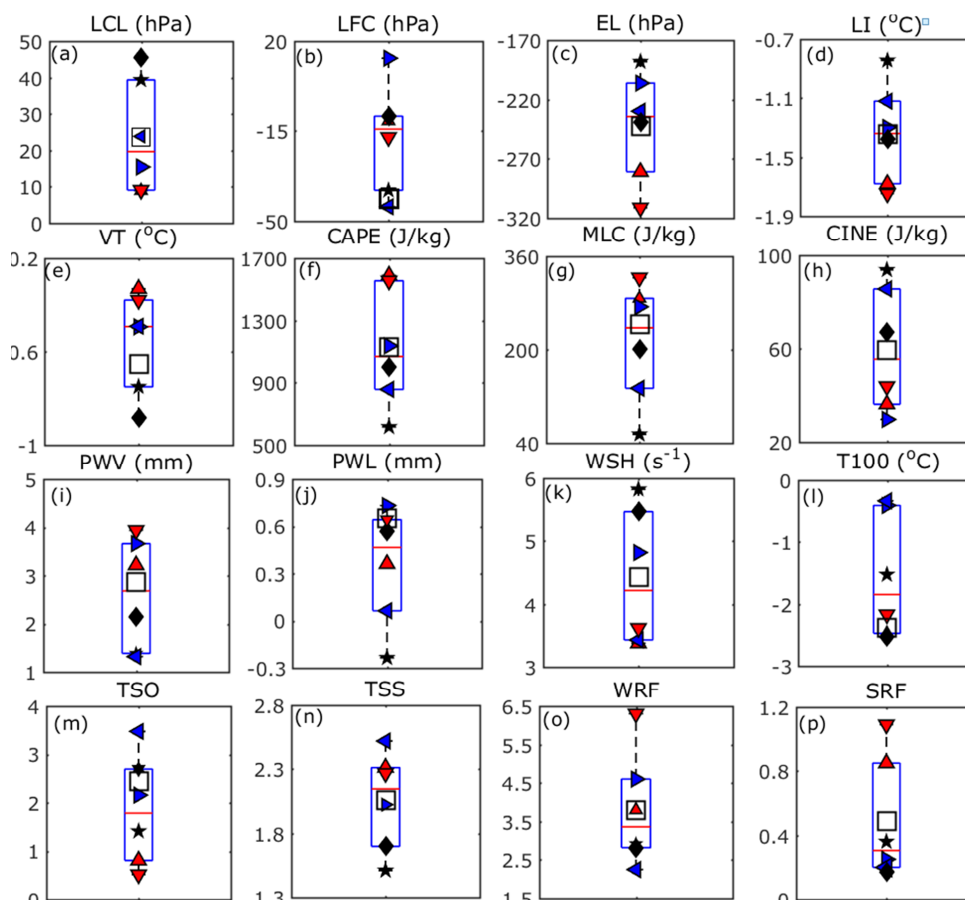
Figure 5: Long-term variation of (a) LCL, (b) LFC, (c) EL, (d) LI, (e) VT, (f) CAPE, (g) MLC, (h) CINE, (i) PWV, (j) PWL, (k) WSH, (l) T100, (m) TSO, (n) TSS, (o) WRF and (p) SRF over the six sub-divisions of India during the period 1980-2016. Legends are same as in Figure 4.
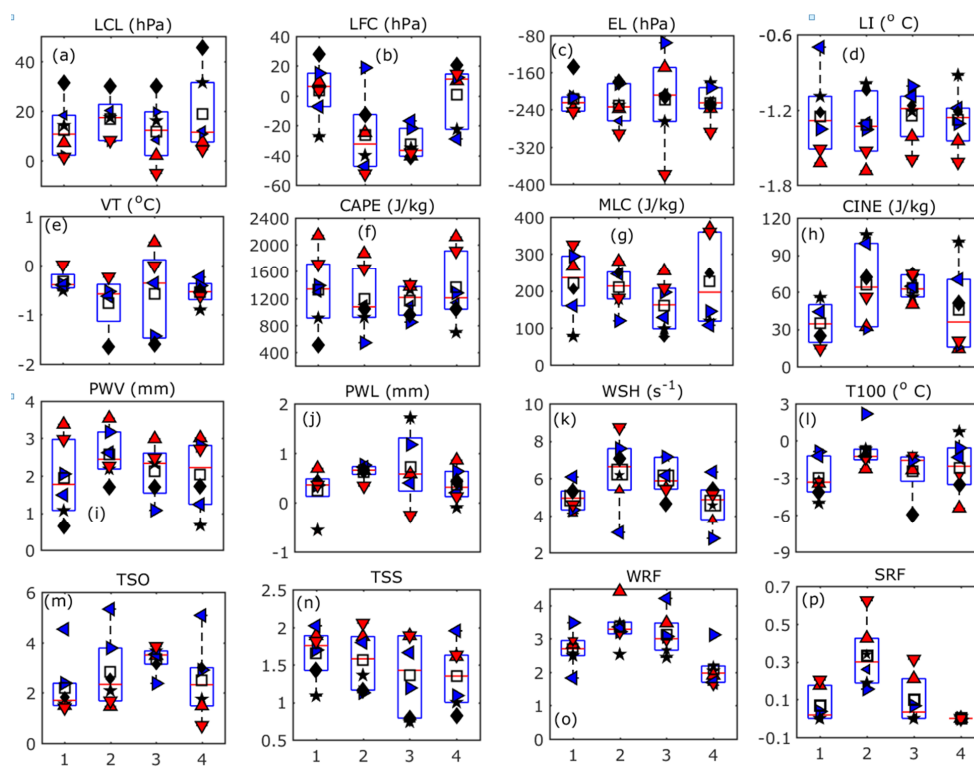
Figure 6: Seasonal trend of (a) LCL, (b) LFC, (c) EL, (d) LI, (e) VT, (f) CAPE, (g) MLC, (h) CINE, (i) PWV, (j) PWL, (k) WSH, (l) T100, (m) TSO, (n) TSS, (o) WRF and (p) SRF over India during all seasons. Here 1 refers to pre-monsoon (March-May), 2 refers to Monsoon (June-September), 3 for Post-monsoon (October-November) and 4 for Winter (December-February) Legends are same as in Figure 4.
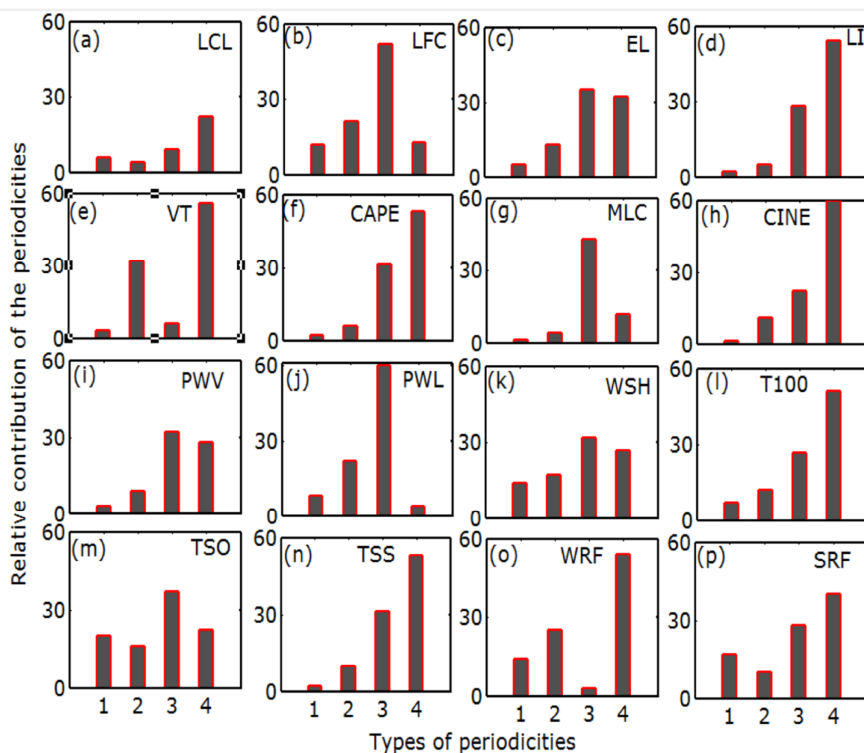
Figure 7: Percentage contribution of various periodicities on long-term trend of all instability parameters over India namely: 1.5 -2.5 years periodicity denoted as 1, 4 -6 years periodicity denoted as 2, 10-12 years periodicity displayed as 3 and 16 – 20 years periodicity represented as 4.
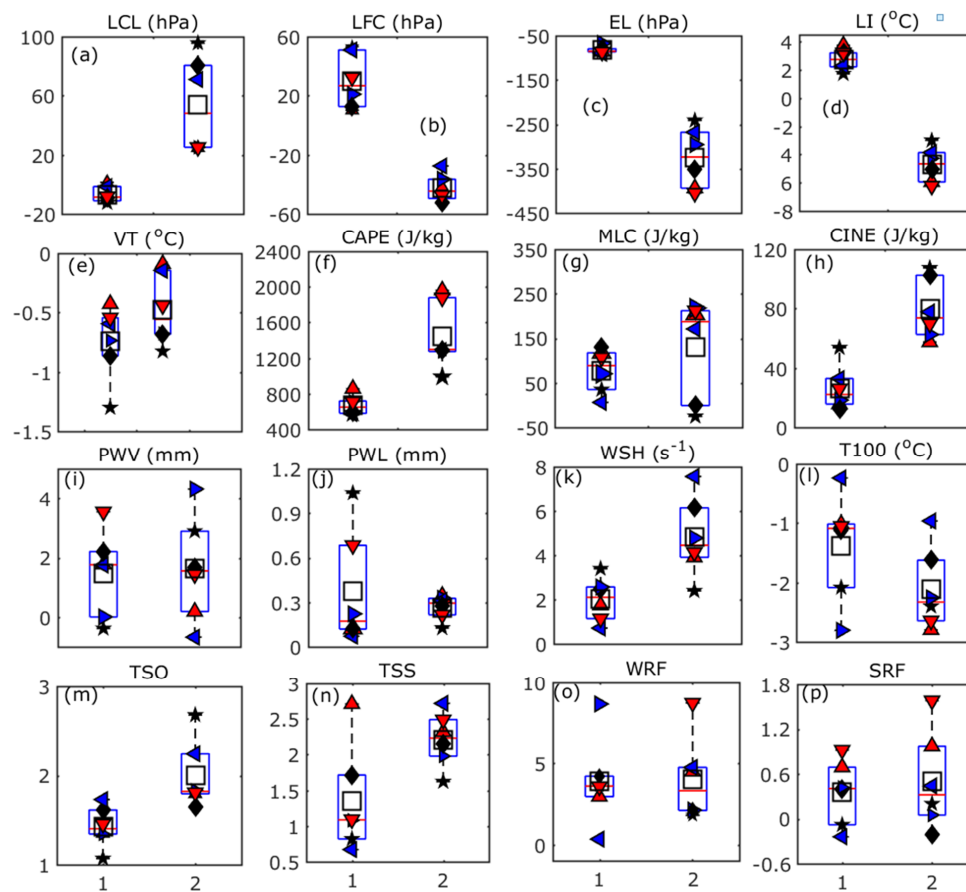
Figure 8: Average long-term trends of various instability parameters over the six sub-divisions of India in two half periods of 18 years each (1 represents   first half period C1 during 1980-1997 and 2 showing second half period C2) during 1999-2016. Legends are same as in Figure 4.
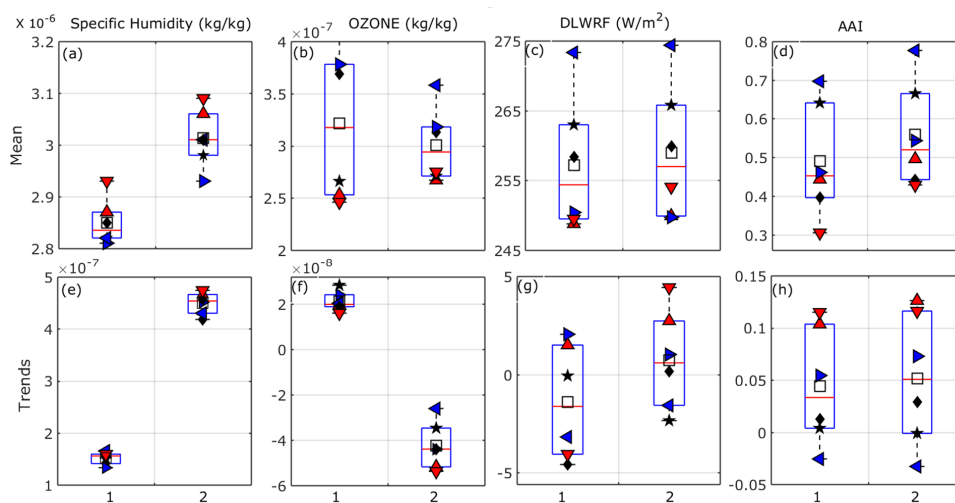
Figure 9: Average and climatological trends of specific humidity, ozone mixing ratio at 100 hPa and Downward Longwave radiation flux with Absorptive Aerosol Index over the six sub-divisions of India over two half periods of 18 years each (1980-1997 and 1999-2016). Legends are same as in Figure 4.

Appendix

Table A1: Details of the dataset used.

Serial no.	Station no.	Latitude	Longitude	Station Name	No. of profiles available	No. of profiles utilized	Region
1	42361	26.23	78.25	Gwalior	9901	9412	Central India
2	42369	26.75	80.88	Lucknow	16869	16387	
3	42379	26.75	83.37	Gorakhpur	12376	11793	
4	42667	23.28	77.35	Bhopal	14795	13968	
5	42809	22.65	88.45	Kolkata	15212	14626	Eastern Coasts
6	42971	20.25	85.83	Bhubaneshwar	18325	17552	
7	43150	17.68	83.3	Vishakhapatnam	13225	12856	
8	43185	16.2	81.15	Machilipatnam	17108	16374	
9	43279	13	80.18	Chennai	14067	13487	
10	43346	10.92	79.83	Karaikal	16519	16106	
11	42314	27.48	95.02	Dibrugarh	10067	9550	North Eastern
12	42410	26.1	91.58	Guwahati	15280	14803	
13	42492	25.6	85.17	Patna	8934	8318	
14	42724	23.88	91.25	Agartala	15234	14732	
15	42101	30.33	76.47	Patiala	11572	10129	North Western
16	42182	28.58	77.2	New	14077	13982	
17	42339	26.3	73.02	Jodhpur	13133	12918	
18	42647	23.06	72.63	Ahmadabad	11430	11006	
19	42867	21.1	79.05	Sonegaon	15626	14971	Peninsular India
20	43014	19.85	75.4	Aurangabad	14220	13993	
21	43041	19.08	82.03	Jagdalpur	10568	10205	
22	43128	17.45	78.47	Hyderabad	10234	9723	
23	43295	12.97	77.58	Bangalore	10150	9514	
24	43003	19.12	72.85	Bombay	14102	13808	Western Coasts
25	43192	15.48	73.82	Goa	7070	6313	
26	43285	12.95	74.83	Mangalore	9866	9406	
27	43371	8.48	76.95	Thiruvananthapuram	11590	11120	

Table A2: List of Abbreviations

Slno.	Abbreviation	Full Form
1	LCL (hPa)	Lifted Condensation Level
2	LFC (hPa)	Level of Free Condensation
3	EL (hPa)	Equilibrium Level
3	LI (^{o}C)	Lifted Index
4	VT (^{o}C)	Vertical Totals Index
5	CAPE (J/kg)	Convective Available Potential Energy
6	MLC (J/kg)	Mixed Layer CAPE
7	CINE (J/kg)	Convective Inhibition
8	PWV (mm)	Precipitable Water Vapour
9	PWL (mm)	Lower Level PWV
10	WSH (s^{-1})	Wind Shear
11	T100 (^{o}C)	Temperature at 100 hPa
12	TSO	Ordinary Thunderstorm Frequency
13	TSS	Severe Thunderstorm Frequency
14	WRF	Weak Rainfall Frequency
15	SRF	Severe Rainfall Frequency
16	SHUM (kg/kg)	Specific humidity
17	AAI	Absorptive Aerosol Index
18	IMD	India Meteorological Department
19	IGRA	Integrated Global Radiosonde Archive
20	GHG	Green House Gas
21	DLWRF (W/m^2)	Downward Long Wave Radiation Flux
22	EMD	Empirical Mode Decomposition
23	UTLS	Upper Troposphere Lower Stratosphere
24	QBO	Quasi-biennial oscillation
25	ENSO	El Niño–Southern Oscillation